Thakur Pankaj, Pawan Kumar, Priya Gulial*

THERMAL AND MECHANICAL LOAD RESPONSE OF BRAKE DISCS WITH RIGID SHAFTS: A COMPARATIVE ANALYSIS OF CAST IRON AND STAINLESS STEEL

ODZIV TERMIČKOG I MEHANIČKOG OPTEREĆENJA KOČIONIH DISKOVA NA KRUTIM OSOVINAMA: UPOREDNA ANALIZA LIVENOG GVOŽĐA I NERĐAJUĆEG ČELIKA

Originalni naučni rad / Original scientific paper
Rad primljen / Paper received: 17.04.2025
https://doi.org/10.69644/ivk-2026-01-0131

Adresa autora / Author's address:
Department of Mathematics, Faculty of Science & Technology, ICFAI University, Himachal Pradesh, India

*email: pankaj_thakur15@yahoo.co.in
P. Thakur https://orcid.org/0000-0001-8119-2697
P. Gulial https://orcid.org/0009-0009-0266-2298

Keywords

- thermal load
- rigid shaft
- brake disc
- material comparison
- mechanical load

Ključne reči

- termičko opterećenje
- kruta osovina
- kočioni disk
- poređenje materijala
- mehaničko opterećenje

Abstract

This study examines the performance of cast iron and stainless steel brake discs under varying loads and temperatures, with a focus on angular speed, radial stress, and circumferential stress. The results show that angular speed decreases with higher radii ratios and loads for both materials, with cast iron outperforming stainless steel due to its lower density and higher stiffness. Stainless steel exhibits higher radial stress and greater sensitivity to temperature changes. Circumferential stress decreases with the radii ratio, with stainless steel consistently showing higher stress levels, particularly at higher loads. Overall, cast iron is more efficient in maintaining angular speed, while stainless steel is more sensitive to stress and temperature variations.

Izvod

U ovom radu istražujemo performanse kočionih diskova od livenog gvožđa i nerđajućeg čelika u uslovima promenljivog opterećenja i temperature, sa fokusom na ugaonu brzinu, radijalni napon i obimski napon. Rezultati pokazuju da ugaona brzina opada sa povećanjem odnosa poluprečnika i sa opterećenjem kod oba materijala, gde liveno gvožđe pokazuje bolje osobine u odnosu na nerđajući čelik, usled njegove manje gustine i veće krutosti. Nerđajući čelik ispoljava veći radijalni napon i veću osetljivost na promenu temperature. Obimski napon opada sa odnosom poluprečnika, gde nerđajući čelik pokazuje veće vrednosti napona, posebno kod većih opterećenja. U opštem slučaju, liveno gvožđe je efikasnije u održavanju ugaone brzine, dok je nerđajući čelik osetljiviji prema promeni napona i temperature.

INTRODUCTION

Brake discs are essential components in various mechanical systems, especially in high-performance applications such as railway and automotive braking systems. The discs, mounted on sturdy shafts, are subjected to both heat and mechanical forces during braking. Zenkour et al. /1/ investigate elastic deformation in rotating functionally graded material (FGM) discs. Zenkour focuses on radially graded discs with rigid casing, while Chen et al. /2/ extend to three-dimensional, transversely isotropic FGMs. Both studies provide analytical solutions crucial for optimising high-speed rotating machinery designs. Chen et al. /2/ present a three-dimensional analytical solution for stress and deformation in rotating FGM discs with transverse isotropy. Their study considers radial material gradation and anisotropy, offering critical insights for optimising high-performance mechanical systems like aerospace and rotating machinery components. Bayat et al. /3/ analyse functionally graded rotating discs with variable thickness, focusing on stress distribution and deformation. Using analytical and numerical methods, the study highlights the effects of material gradation and disc geometry on performance, offering valuable insights for optimising designs in high-speed applications like turbines and flywheels. Additionally, Bayat et al. /4/ investigate mechanical and thermal stresses in functionally graded rotating discs with variable thickness under radially symmetric loads. Their study combines analytical and numerical approaches to examine the interplay of material gradation, thermal effects, and geometry, providing critical insights for enhancing the reliability of high-speed rotating systems. Çallıoğlu et al. /5/ analyse stress in functionally graded rotating discs using both analytical and numerical solutions. Their work examines material gradation effects on stress distribution, offering valuable insights for designing efficient and durable high-speed rotating components in engineering applications such as turbines and flywheels. Damircheli et al. /6/ study the impact of temperature and thickness variations on thermal and mechanical stresses in rotating functionally graded discs. Their analysis highlights how material gradation, thermal conditions, and geometry influence stress distribution, providing key insights for optimising the design of high-performance rotating systems in diverse environments. Hassani et al. /7/ present semi-exact elastic solutions for the thermo-mechanical analysis of functionally graded rotating discs. Their study considers material gradation and coupled ther-

mal-mechanical effects, providing accurate stress and deformation predictions. The findings contribute to the design of efficient, high-performance rotating components under complex thermal and mechanical loading conditions. Meanwhile, Dai et al. /8/ examine the mechanical behaviour of a rotating FGM circular disc under variable angular speed. Their study analyses stress and deformation effects influenced by angular acceleration and material gradation, offering insights for optimising dynamic performance in advanced rotating systems like turbines and flywheels. Lin et al. /9/ perform an elastic analysis of rotating functionally graded annular discs with an exponentially varying material profile. Their study investigates the effects of material gradation on stress and deformation, providing valuable insights for the design of high-performance rotating components under complex loading conditions. Farukoğlu et al. /10/ investigate the elastic limit stresses and failure of rotating fibre-reinforced composite discs with variable thickness. Their study examines how material properties, thickness variation, and rotational speed affect the failure criteria, providing critical insights for designing reliable composite components in rotating machinery. Bagheri et al. /11/ present a small-scale oriented elasticity model for functionally graded rotating micro-discs with varying angular velocity, using strain gradient theory. Their study explores the impact of microstructural effects on stress and deformation, providing valuable insights into the behaviour of FG micro-discs in advanced mechanical systems. Babaei et al. /12/ explore the dynamic behaviour of functionally graded truncated cones under rotational motion. The study incorporates the effects of porous material saturation, providing insights into their mechanical properties and stability under rotational loading conditions. Liu et al. /13/ investigate a rare hyperluminous rotating disc galaxy observed through an Einstein ring. The study, based on data from advanced telescopes, sheds light on the galaxy's properties and its role in the early universe, offering new insights into the formation and evolution of massive galaxies 10 billion years ago. Alfredsson et al. /14/ undertook a comprehensive review of the fluid dynamics associated with rotating discs and cones. The study covers the underlying physical mechanisms, mathematical modelling, and experimental observations related to flow behaviour in these configurations, with applications ranging from industrial processes to fundamental fluid dynamics research. Furthermore, Aziz et al. /15/ explore the enhancement of the load-bearing capabilities of hollow rotating discs. The authors investigate the effects of rotational autofrettage, a process that involves inducing compressive residual stresses, on the structural integrity and strength of these discs under rotational loading. The study provides valuable insights for engineering applications requiring high-performance rotating components. The study by Afzal and Abdul /16/ reviews the thermo-mechanical and structural performance of automobile disc brakes, highlighting both numerical and experimental studies. It discusses various materials' thermal conductivity, mechanical properties, wear resistance, and fatigue behaviour under braking conditions, providing insights for optimising brake disc design and performance. Borawski's /17/ review explores both conventional and unconventional materials used in the production of brake pads. It examines the advantages and limitations of various materials, including their thermal and mechanical properties, wear resistance, and performance under different braking conditions. The study provides valuable insights for selecting optimal materials for brake pad manufacturing. Chen et al. /18/ discuss the structural design of a high-performance WBD (Water-Cooled Brake Disc). Their study focuses on optimising thermal and mechanical performance, material selection, and thermal management. The research provides valuable insights for enhancing the efficiency, durability, and overall performance of high-performance brake discs. Moreover, Deressa and Ambie /19/ provide a systematic review of thermal load simulations in railway disc brakes. Their study focuses on modelling temperature, stress, and fatigue in braking systems. The review highlights various simulation methods used to predict thermal and mechanical performance, offering insights into optimising brake disc design and improving durability under operational conditions. Additionally, Sumit et al. /20/ conduct a comparative study on the thermal and dynamic analysis of a disc brake using ANSYS® software. The study focuses on evaluating the thermal distribution, stress, and deformation of disc brakes under dynamic loading conditions, providing insights into improving brake performance and design optimisation. Furthermore, Kaur et al. /21/ investigate heat-driven stress in solid discs with varying densities, analysing thermal dynamics to enhance the understanding of material behaviour under thermal loads. Xia et al. /22/ investigate the natural mode behaviour of rotating discs submerged in water at varying wall distances. The study models the dynamics of high-head Francis turbines, focusing on mode splitting and its implications for turbine performance and stability under different operating conditions. Moreover, Gulial et al. /23/ explore how variations in material density influence the strain rates in pressurised rotating cylinders. The study provides critical insights into the mechanical behaviour of such systems, offering implications for engineering applications where material properties and rotational stress are significant factors in design and performance analysis.

Objective of the study

This study examines the thermal and mechanical load responses of rigid shaft brake discs made from cast iron and stainless steel. It analyses heat dissipation, temperature distribution, and mechanical stress under operational conditions, comparing the durability and performance of both materials. The research provides insights into the interaction between the brake disc and shaft, helping optimise material selection and design for improved reliability in high-performance braking systems.

Novelty of this research

The novelty of this research lies in its comprehensive comparison of cast iron and stainless steel brake discs, focusing on their thermal and mechanical load responses in rigid shaft systems. While both materials are widely used in braking applications, this study provides a detailed analysis of their behaviour under dynamic thermal and mechanical stresses, which is crucial for optimising braking performance.

By exploring the interaction between the disc and shaft, the research offers new insights into material efficiency, wear resistance, and system-level performance. The findings aim to enhance the design and longevity of brake discs in high-demand industrial applications.

METHODOLOGY

Seth's /24-25/ and Thakur et al. /26-41/ transition theory is a framework for understanding material behaviour under varying thermal and mechanical conditions. Key points of the methodology include:

- *material state transitions*: it models the transition between different material states, influenced by temperature and mechanical loading;
- *thermal and mechanical interactions*: the theory examines how heat and external loads affect material properties like stiffness, strength, and thermal expansion;
- *application to rotating systems*: it is used to analyse rotating systems, such as discs, to assess performance under changing conditions;
- *predictive modelling*: the theory predicts the impact of temperature and load variations on angular speed, stress, and overall system performance.

CONVERGENCE CRITERIA

The convergence criteria for Seth's transition theory can be summarised as follows:

- *material property stabilisation*: transition between material states (stiffness, strength) stabilises after iterations;
- *residual error*: difference between successive iterations of key variables (stress, angular speed) falls below a set threshold;
- *thermo-mechanical consistency*: predicted stress, angular speed, and thermal responses become consistent;
- *steady-state condition*: key variables reach stable values, indicating a converged solution;
- *physical validity*: results adhere to known material properties and thermodynamics.

ILLUSTRATION OF THE DOMAIN

Geometry of the disc: a thin annular disc composed of cast iron (CI) and stainless steel (SS), with uniform density, is considered for analysis. The disc has a central bore radius a, and an outer radius b, as depicted in Fig. 1. It rotates at a constant angular velocity around an axis perpendicular to its plane while experiencing edge loading. The disc's constant and small thickness ensures a plane stress condition, effectively neglecting axial stress (τ_{zz}). The temperature at the central bore of the disc is denoted by Θ_0.

Boundary conditions: the given boundary conditions describe a system with specific constraints at two radial locations, $r = a$ and $r = b$. At the inner radius ($r = a$): the displacement u is zero, indicating that the point at this radial position is fixed, and the temperature (or scalar field) Θ is set to a constant value Θ_0. At the outer radius ($r = b$): the radial stress τ_{rr} is equal to l_0, representing an applied load at this boundary, while the temperature Θ is set to zero.

The temperature distribution between $r = a$ and $r = b$ follows a logarithmic relation given by $\Theta = \Theta_0 \ln(r/b)/\ln(a/b)$, ensuring that $\Theta = \Theta_0$ at $r = a$ and $\Theta = 0$ at $r = b$.

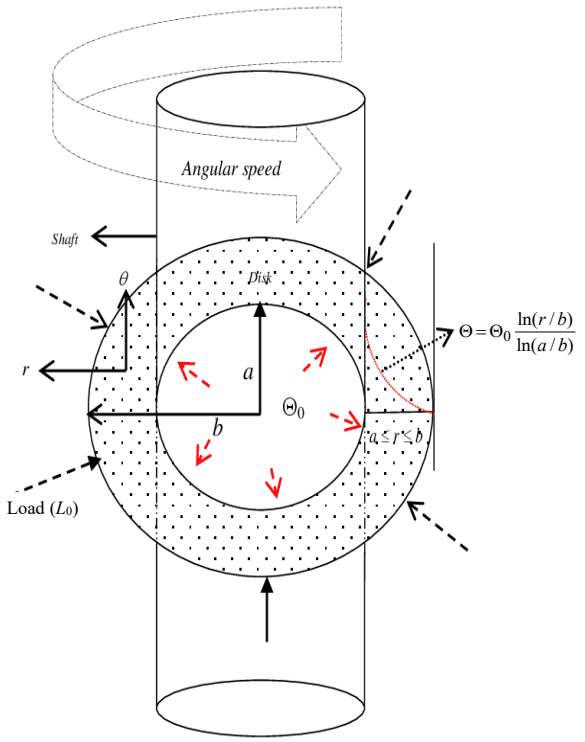

Figure 1. Geometry of the disc.

CONSTITUTIVE EQUATIONS

The stress equation, as described by Gupta et al. /26/, is given by:

$$\tau_{rr} = \frac{2\mu}{n}\left[3-2c-\beta^n\left\{1-c+(2-c)(P+1)^n+\frac{nc\xi\Theta}{2\mu\beta^n}\right\}\right],$$

$$\tau_{\theta\theta} = \frac{2\mu}{n}\left[3-2c-\beta^n\left\{2-c+(1-c)(P+1)^n+\frac{nc\xi\Theta}{2\mu\beta^n}\right\}\right],$$

$$\tau_{r\theta}=\tau_{\theta z}=\tau_{zr}=\tau_{zz}=0\,, \qquad (1)$$

where: $c = 2\mu/\lambda + 2\mu$. Here, all equilibrium conditions are satisfied except:

$$\frac{d}{dr}(r\tau_{rr})-\tau_{\theta\theta}+\rho\omega^2r^2=0\,. \qquad (2)$$

By substituting Eq.(1) and the boundary condition in the previous section into Eq.(2), a nonlinear differential equation is derived as follows:

$$(2-c)n\beta^{n+1}P(P+1)^{n-1}\frac{dP}{d\beta}=\frac{n\rho\omega^2r^2}{2\mu}-\frac{nc\xi\bar{\Theta}_0}{2\mu}+$$
$$+\beta^n\left[1-(P+1)^n-nP\{1-c+(2-c)(P+1)^n\}\right], \qquad (3)$$

where: $\bar{\Theta}_0 = \Theta_0/\ln(a/b)$. In this equation, the turning points of β are identified as $P = -1$ and $\pm\infty$.

INNOVATION

It has been shown /21, 24-41/ that the asymptotic solution for the principal stress undergoes a transition from elastic state to plastic state at transition point P. The transition function χ is defined as follows:

$$\chi=\frac{n}{2\mu}[\tau_{\theta\theta}-c\xi\Theta]=(3-2c)-\beta^n\{2-c+(1-c)(P+1)^n\}-\frac{nc\xi\Theta}{\mu}. \qquad (4)$$

By logarithmically differentiating Eq.(4) with respect to r and substituting the value of $dP/d\beta$ from Eq.(3), we get:

$$\frac{d(\log\chi)}{dr}=-\frac{\beta^n\left(\frac{1-c}{2-c}\right)\left[1-(P+1)^n-n(1-c)P+\frac{n\rho\omega^2r^2}{2\mu\beta^n}+\frac{nc\xi\bar{\Theta}_0(3-2c)}{\mu(4-2c)\beta^n}\right]+(2-c)nP\beta}{r\left[3-2c-\beta^n\{2-c+(1-c)(P+1)^n\}-\frac{nc\xi\Theta}{2\mu}\right]}. \tag{5}$$

Taking the asymptotic value P from Eq.(5) and integrating, we obtain the following:

$$\chi=k_1r^{\nu-1}, \tag{6}$$

where: $\nu=(1-c)/(2-c)$. From Eqs.(4) and (6), we derive:

$$\tau_{\theta\theta}=\left(\frac{2\mu}{n}\right)K_1r^{\nu-1}+\frac{c\xi\Theta_0\ln(r/b)}{\log(a/b)}. \tag{7}$$

By substituting Eq.(7) into Eq.(2) and performing the integration, we obtain:

$$\tau_{rr}=\frac{2\mu}{n\nu}k_1r^{\nu-1}+\frac{c\xi\Theta_0\log(r/b)}{\ln(a/b)}-\frac{c\xi\Theta_0}{\ln(a/b)}-\frac{\rho\omega^2r^2}{3}+\frac{k_2}{r}. \tag{8}$$

By substituting Eqs.(7) and (8) into the relation $1-\beta^2=(2/E)[\tau_{\theta\theta}-\nu\tau_{rr}]+\alpha\Theta$, provided by Gupta et al. /26/, we get:

$$\beta=\sqrt{1-\frac{2\nu}{E}\left(\frac{\rho\omega^2r^2}{3}-\frac{k_2}{r}+\frac{c\xi\Theta_0}{\ln(a/b)}\left[1+\frac{2\ln(r/b)}{(1-c)}\right]\right)}.$$

Substituting the value of β into $u=r(1-\beta)$ as given by Gupta et al. /26/, we get:

$$u=r\left[1-\sqrt{1-\frac{2\nu}{E}\left(\frac{\rho\omega^2r^2}{3}-\frac{K_2}{r}+\frac{\alpha E(2-c)\Theta_0}{\ln(a/b)}\left[1+\frac{2\ln(r/b)}{(1-c)}\right]\right)}\right], \tag{9}$$

where: $c\xi=\alpha E(2-c)$. Using boundary condition (section *Illustration of the domain*) in Eqs.(8) and (9), we get:

$$k_1=\frac{n\nu}{2\mu b^\nu}\left[bl_0+\frac{\rho\omega^2(b^3-a^3)}{3}\right]+\frac{\alpha E\Theta_0}{\mu b^\nu}\left[\frac{(1-c)(b-a)-2na\ln(a/b)}{2\ln(a/b)}\right] \quad \text{and} \quad k_2=\frac{\rho\omega^2a^3}{3}+\frac{\alpha E\Theta_0(2-c)}{\ln(a/b)}\left[\frac{(1-c)-2\ln(r/b)}{(1-c)}\right].$$

Substituting the values of constants k_1 and k_2 from Eqs.(17), (18), and (20), we derive the following:

$$\sigma_\theta=\nu(1-R_0^3)R^\nu\frac{\Omega_i^2}{3R}+\nu L_0R^{\nu-1}+\frac{\Theta_1}{(1-\nu)}\left[\frac{R^\nu(1-R_0)\nu}{\ln R_0.R}+\frac{\ln R}{\ln R_0}-2R_0(1-\nu)R^{\nu-1}\right], \tag{10}$$

$$\sigma_r=\frac{\Omega_i^2}{3R}\left[R^\nu(1-R_0^3)-R^3+R_0^3\right]+L_0R^{\nu-1}+\frac{2R_0\Theta_1(1-R^\nu)}{\nu R}+\frac{\Theta_1(1-R^\nu)}{(1-\nu)\ln R_0}\left[\ln R+\frac{(1-R_0)}{R}R^\nu+\frac{R_0}{R}-1\right], \tag{11}$$

$$U=R-R[1-2\nu H]\left\{\frac{\Omega_i^2}{3R}[R^3-R_0^3]+\frac{2\Theta_1(R-R_0)}{R\ln R_0(1-\nu)}+\frac{2\Theta_1}{\nu}\left[\frac{\ln R}{\ln R_0}-\frac{R_0}{R}\right]\right\}, \tag{12}$$

where: $1-c=(1-\nu)/\nu$; $L_0=l_0/Y$; $R=r/b$; $R_0=a/b$; $\sigma_r=\tau_{rr}/Y$; $\sigma_\theta=\tau_{\theta\theta}/Y$; $\Theta_1=\alpha E\Theta_0/Y_1$; $H=Y/E$; and $\Omega^2=\rho_0\omega^2b^2/Y$.

Initial yielding: from Eqs.(10) and (11), it is evident that the value $\tau_{rr}-\tau_{\theta\theta}$ is maximal at the internal surface (i.e., at $R=R_0$). Hence, yielding will occur at the internal surface of the disc. The angular velocity required for the onset of yielding is expressed as:

$$\Omega^2\Big|_{\text{initial yielding surface}}=\left|\frac{3}{(1-R_0^3)}\left[\frac{R_0^{\nu-1}}{(1-\nu)}-\sigma_0\right]\right|-\left|\frac{3\Theta_1}{(1-R_0^3)(1-\nu)}\left[\frac{1-R_0}{\ln R_0}-\frac{2}{\nu}\{R_0^{1-\nu}-(1-\nu)R_0\}\right]\right|. \tag{13}$$

For the fully plastic state, Eqs.(10)-(13) become:

$$\sigma_\theta=\frac{\Omega_i^2(1-R_0^3)\sqrt{R}}{6R}+\frac{L_0}{2\sqrt{R}}+2\Theta_1\left[\frac{\sqrt{R}(1-R_0)}{2\ln R_0.R}+\frac{\ln R}{\ln R_0}-\frac{R_0}{\sqrt{R}}\right], \tag{14}$$

$$\sigma_r=\frac{\Omega_i^2}{3R}[\sqrt{R}(1-R_0^3)-R^3+R_0^3]+\frac{L_0}{\sqrt{R}}+\frac{4R_0\Theta_1(1-\sqrt{R})}{R}+\frac{2\Theta_1(1-\sqrt{R})}{\ln R_0}\left[\ln R+\frac{(1-R_0)}{R}\sqrt{R}+\frac{R_0}{R}-1\right], \tag{15}$$

$$U=R-R[1-H]\left\{\frac{\Omega_i^2}{3R}[R^3-R_0^3]+\frac{4\Theta_1(R-R_0)}{R\ln R_0}+4\Theta_1\left[\frac{\ln R}{\ln R_0}-\frac{R_0}{R}\right]\right\}, \tag{16}$$

and

$$\Omega^2\Big|_{\text{fully plastic surface}}=\left|\frac{3}{(1-R_0^3)}\left[\frac{2}{\sqrt{R_0}}-L_0\right]\right|-\left|\frac{6\Theta_1}{(1-R_0^3)}\left[\frac{1-R_0}{\ln R_0}-4\left\{\frac{1}{\sqrt{R_0}}-\frac{R_0}{2}\right\}\right]\right|. \tag{17}$$

VERIFICATION OF RESULTS

Results derived from Eqs.(10)-(13) for initial yielding and from Eqs.(14)-(17) for the fully plastic state under thermo-mechanical load are consistent with those reported by Gupta et al. /26/, although their study did not account for load parameters. This alignment reinforces the validity of the obtained outcomes in relation to existing literature.

NUMERICAL SIMULATION

To calculate thermal stress distribution, angular speed, and displacement, we consider the properties of the materials and their conditions. For cast iron (CI), the Poisson's ratio $\nu=0.25$ and stainless steel (SS) $\nu=0.31$; $E/Y=2$, 1/2; load $L_0=0$, 1, 2; temperature $\Theta_1=0$ and 0.35, which affects the thermal expansion of the material. By applying these values

to appropriate Eqs.(10)-(13) for thermal stress, angular speed, and displacement, we can assess the materials' behaviour under different loads, temperatures, and deformations. This method allows us to better understand how these factors interact and affect the material's performance. Curves illustrating the relationship between angular speed required for initial yielding and various radius ratios (R_0) for disc brakes made of cast iron (CI) and stainless steel (SS) under varying loads (L_0 = 1 and 2) at temperatures (Θ_1 = 0 and 0.35) are presented in Fig. 2. It has been observed that angular speed consistently decreases with increasing radius ratio and load for both materials. At a temperature of Θ_1 = 0, the angular speed is higher across all conditions, while at Θ_1 = 0.35, there is a noticeable reduction in angular speed, particularly at higher radius ratios and loads. This reduction can be attributed to the combined effects of increased frictional forces, thermal expansion, and potential softening of materials at elevated temperatures. The cast iron disc brake demonstrates better angular speed performance compared to the stainless steel disc brake under the same conditions, likely due to its lower density and higher stiffness, which enable it to sustain rotational motion more effectively. The influence of load is significant, with angular speed dropping sharply as the load increases from 0 to 2, especially for the stainless steel disc brake. At higher radius ratios, both materials exhibit a convergence toward a minimum angular speed, suggesting a natural limit to rotational efficiency as the distance from the axis of rotation increases. This is particularly evident at Θ_1 = 0.35, where the decline in angular speed is steeper, indicating a greater loss of rotational energy at higher temperatures. Overall, the results emphasise the intricate interplay between temperature, load, material properties, and radius ratio on rotational dynamics. The cast iron disc brake emerges as the more efficient material for maintaining angular speed under increasing load and temperature, while the stainless steel disc brake exhibits greater sensitivity to these factors.

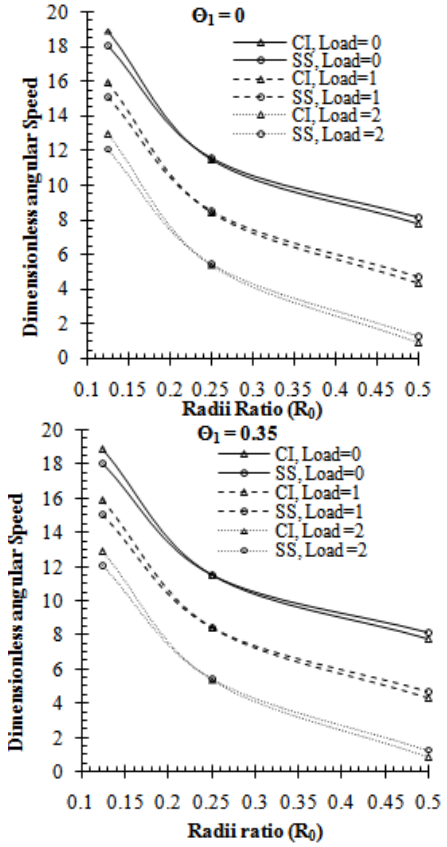

Figure 2. Dimensionless angular speed vs. radii ratio (R_0).

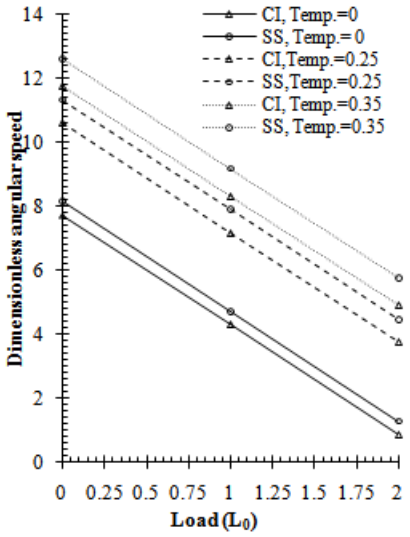

Figure 3. Dimensionless angular speed vs. load (L_0).

Figure 3 demonstrates the relationship between dimensionless angular speed and load (L_0) for disc brakes of CI and SS at temperatures (Θ_1 = 0, 0.25, and 0.35). As the load increases, angular speed decreases for both materials, following a linear pattern. Interestingly, SS disc brakes consistently maintain higher angular speeds than CI disc brakes, suggesting that SS offers superior rotational performance. However, as temperature increases, angular speed also increases for both materials, indicating that heat influences performance, likely due to reduced friction or material softening. The reduction in angular speed is more pronounced in SS, highlighting its greater sensitivity to both temperature and load variations.

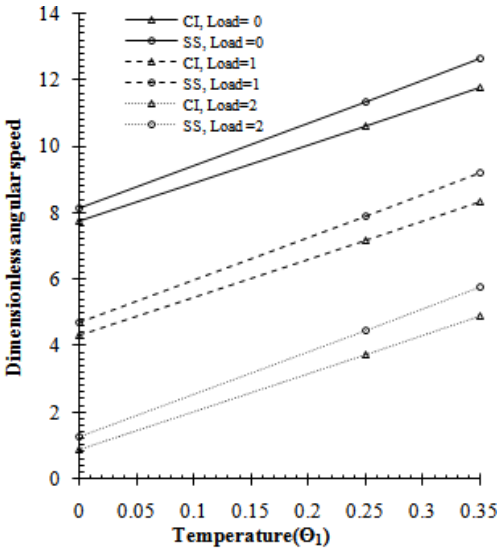

Figure 4. Dimensionless angular speed vs. temperature (Θ_1).

Figure 4 illustrates the variation in dimensionless angular speed with temperature (Θ_1) for disc brakes made of CI and SS under loads (L_0 = 0, 1, and 2). The dimensionless angular speed increases with temperature for both materials, but the SS disc brake consistently achieves higher angular speeds than the CI disc brake across all loads. Higher loads result in lower angular speeds, with the gap between SS and CI widening as the load increases. This trend suggests that SS is more efficient at maintaining rotational performance under both thermal effects and load. The linear increase in angular speed with temperature indicates improved system dynamics despite the added thermal influence.

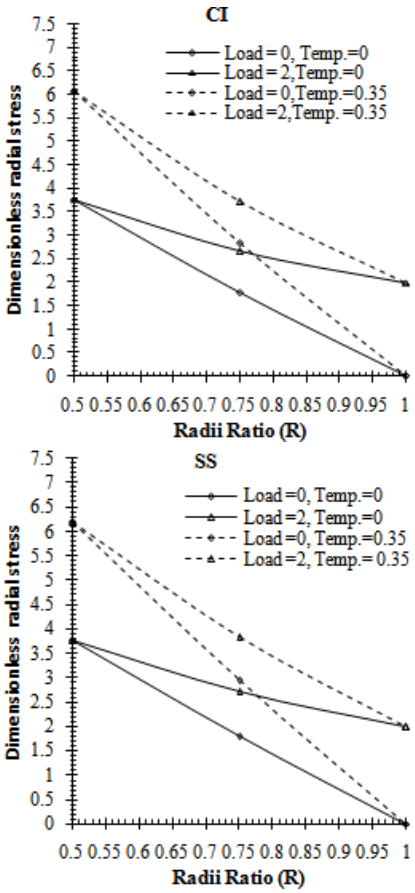

Figure 5. Dimensionless radial stress vs. radii ratio (R).

Figure 5 depicts the behaviour of dimensionless radial stress distribution as a function of radius ratio (R) for disc brakes made of CI and SS under different loading conditions (L_0 = 0 and 2) and temperatures (Θ_1 = 0 and 0.35). As the radius ratio (R) increases, radial stress clearly decreases for both materials. However, SS disc brake consistently shows higher stress compared to the CI one, mainly because of its stronger elastic modulus. Mechanical loading plays a key role in radial stress, with a load of L_0 = 2 causing more stress than L_0 = 0, especially at smaller radius ratios. As temperature increases to Θ_1 = 0.35, radial stress rises for both materials, but the increase is more noticeable in SS, suggesting it is more affected by temperature changes than CI. The CI disc brake, having a higher thermal expansion coefficient, experiences lower stress under the same loading conditions but undergoes more deformation as the temperature changes. On the other hand, the SS disc brake, due to its lower thermal expansion and higher modulus, experiences higher stress, making it more sensitive to temperature variations. These results highlight how mechanical loading and temperature work together to affect radial stress distribution in rotating discs, with SS showing both higher stress and greater temperature sensitivity than CI.

Figure 6 illustrates the dimensionless circumferential stress distribution as a function of radius ratio (R) for disc brakes of CI and SS under loading conditions (L_0 = 0 and 2) and temperature conditions (Θ_1 = 0 and 0.35). In both cases, circumferential stress decreases as radius ratio increases, irrespective of the material, load, or temperature. At Θ_1 = 0, SS exhibits higher stress levels than CI, while the elevated temperature (Θ_1 = 0.35) leads to a noticeable reduction in stress for both materials, indicating a thermal softening effect. The application of L_0 = 2 results in higher circumferential stress compared to L_0 = 0 across all conditions, emphasising the influence of mechanical loading. Despite variations in stress levels due to load and temperature, the trends remain consistent, with SS consistently exhibiting higher stresses than CI under identical conditions.

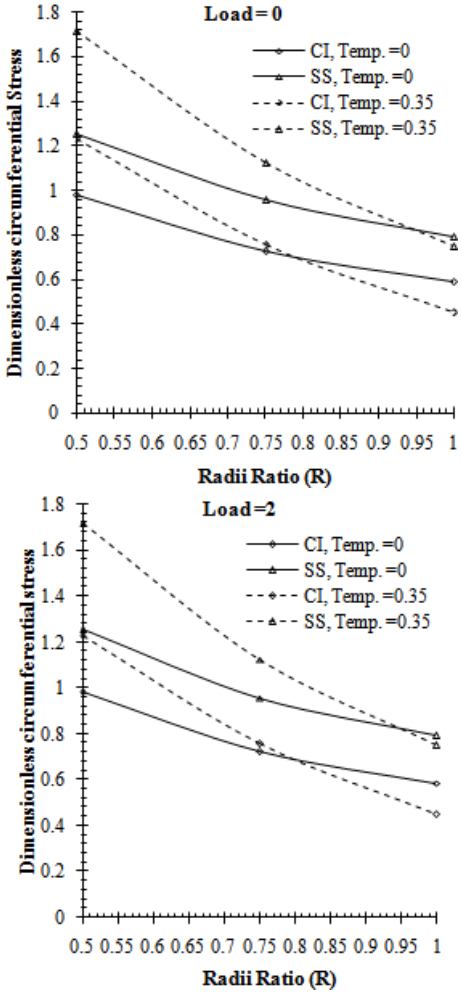

Figure 6. Dimensionless circumferential stress vs. radii ratio (R).

CONCLUSIONS

Comparative analysis of cast iron (CI) and stainless steel (SS) discs under varying thermal and mechanical loads

demonstrates that CI sustains higher angular velocities due to its lower density and superior stiffness properties. Both materials exhibit a decrease in angular speed and an increase in radial and circumferential stresses with rising temperature; however, SS shows greater thermal sensitivity, resulting in more pronounced stress responses. Similarly, increasing mechanical loads lead to a reduction in angular speed and elevated stress levels in both materials, with SS again displaying higher sensitivity to load variations. Under combined thermal and mechanical loading conditions, CI exhibits enhanced performance efficiency and structural stability, whereas SS is characterised by increased stress magnitudes and reduced resistance to thermal effects. This investigation provides a comprehensive comparison of angular velocity, radial stress, and circumferential stress behaviour in CI and SS discs, emphasising the influence of material properties on their dynamic and structural performance.

REFERENCES

1. Zenkour, A.M. (2007), *Elastic deformation of the rotating functionally graded annular disk with rigid casing*, J Mater. Sci. 42 (23): 9717-9724. doi: 10.1007/s10853-007-1946-6
2. Chen, J.-Y., Ding, H.-J., Chen, W.-Q. (2007), *Three-dimensional analytical solution for a rotating disc of functionally graded materials with transverse isotropy*, Arch. Appl. Mech. 77(4): 241-251. doi: 10.1007/s00419-006-0098-5
3. Bayat, M., Saleem, M., Sahari, B.B., et al. (2008), *Analysis of functionally graded rotating disks with variable thickness*, Mech. Res. Comm. 35(5): 283-309. doi: 10.1016/j.mechrescom.2008.02.007
4. Bayat, M., Saleem, M., Sahari, B.B., et al. (2009), *Mechanical and thermal stresses in a functionally graded rotating disk with variable thickness due to radially symmetry loads*, Int. J Pres. Ves. Pip. 86(6): 357-372. doi: 10.1016/j.ijpvp.2008.12.006
5. Çallioğlu, H., Bektaş, N.B., Sayer, M. (2011), *Stress analysis of functionally graded rotating discs: analytical and numerical solutions*, Acta Mech. Sin. 27(6): 950-955. doi: 10.1007/s10409-011-0499-8
6. Damircheli, M., Azadi, M. (2011), *Temperature and thickness effects on thermal and mechanical stresses of rotating FG-disks*, J Mech. Sci. Technol. 25(3): 827-836. doi: 10.1007/s12206-011-0110-z
7. Hassani, A., Hojjati, M.H., Farrahi, G., Alashti, R.A. (2011), *Semi-exact elastic solutions for thermo mechanical analysis of functionally graded rotating disks*, Compos. Struct. 93(12): 3239-3251. doi: 10.1016/j.compstruct.2011.06.001
8. Dai, T., Dai, H.-L. (2015), *Investigation of mechanical behavior for a rotating FGM circular disk with a variable angular speed*, J Mech. Sci. Technol. 29: 3779-3787. doi: 10.1007/s12206-015-0824-4
9. Lin, W.-F. (2020), *Elastic analysis for rotating functionally graded annular disk with exponentially-varying profile and properties*, Math. Probl. Eng. 2020: 2165804. doi: 10.1155/2020/2165804
10. Farukoğlu, Ö.M., Korkut, I. (2021), *On the elastic limit stresses and failure of rotating variable thickness fiber reinforced composite disk*, ZAMM- J Appl. Math. Mech. 101(9): e202000356. doi: 10.1002/zamm.202000356
11. Bagheri, E., Asghari, M., Kargarzadeh, A., Badiee, M. (2021), *Small-scale oriented elasticity modeling of functionally graded rotating micro-disks with varying angular velocity in the context of the strain gradient theory*, Acta Mechanica, 232(6): 2395-2416. doi: 10.1007/s00707-021-02945-2
12. Babaei, M., Asemi, K., Kiarasi, F. (2021), *Dynamic analysis of functionally graded rotating thick truncated cone made of saturated porous materials*, Thin-Walled Struct. 164(1): 107852. doi: 10.1016/j.tws.2021.107852
13. Liu, D., Förster Schreiber, N.M., Harrington, K.C., et al. (2024), *Detailed study of a rare hyperluminous rotating disk in an Einstein ring 10 billion years ago*, Nat. Astron. 8: 1181-1194. doi: 10.1038/s41550-024-02296-7
14. Alfredsson, P.H., Kato, K., Lingwood, R.J. (2024), *Flows over rotating disks and cones*, Annual Rev. Fluid Mech. 56: 45-68. https://doi.org/10.1146/annurev-fluid-121021-043651
15. Aziz, F., Kamal, S.M., Perl, M., Chetry, A. (2024), *Increasing the load carrying capacity of hollow rotating disks by applying rotational autofrettage*, Eur. J Mech. - A/Solids, 105: 105231. doi: 10.1016/j.euromechsol.2024.105231
16. Afzal, A., Abdul Mujeebu, M. (2019), *Thermo-mechanical and structural performances of Automobile disc brakes: A review of numerical and experimental studies*, Arch. Computat. Methods Eng. 26: 1489-1513. doi: 10.1007/s11831-018-9279-y
17. Borawski, A. (2020), *Conventional and unconventional materials used in the production of brake pads - review*, Sci. Eng. Compos. Mater. 27(1): 374-396. doi: 10.1515/secm-2020-0041
18. Chen, A., Kang, K.-J., Kienhöfer, F. (2021), *The structural design of a high-performance WBD brake disc*, R&D J, 37: 70-79. doi: 10.17159/2309 8988/2021/v37a8
19. Deressa, K.T., Ambie, D.A. (2021), *Thermal load simulations in railway disc brake: A systematic review of modelling temperature, stress and fatigue*, Arch. Computat. Methods Eng. 29: 2271-2283. doi: 10.1007/s11831-021-09662-y
20. Sau, S.K., Pulinat, K.G., Moss, P.N., et al. (2022), *A comparative study on the thermal and dynamic analysis of a disc brake using Ansys*, Mater. Today: Proc. 65(8): 3714-3723. doi: 10.1016/j.matpr.2022.06.318.
21. Kaur, J., Singh, N., Thakur P. (2025), *Heat-driven stress: Comprehending thermal dynamics in solid disks with varying different densities*, ZAMM-J Appl. Math. Mech. 105(1): e202401087. doi: 10.1002/zamm.202401087
22. Xia, X., Moraga, G., Presas, A., et al. (2025), *Natural mode splitting of a rotating disc in water at different wall distances as a model for high-head francis runners*, J Sound Vibr. 597 (Part B): 118824. doi: 10.1016/j.jsv.2024.118824
23. Gulial, P., Thakur, P. (2025), *Investigating the effects of material density on strain rates in pressurized rotational cylinders*, ZAMM-J Appl. Math. Mech. 105(2): e202401011. doi: 10.1002/zamm.202401011
24. Seth, B.R. (1962), *Transition theory of elastic-plastic deformation, creep and relaxation*, Nature, 195: 896-897. doi:10.1038/195896a0
25. Seth, B.R. (1966), *Measure-concept in mechanics*, Int. J Non-Linear Mech. 1(1): 35-40. doi: 10.1016/0020-7462(66)90016-3
26. Gupta, S.K., Thakur, P. (2007), *Thermo elastic-plastic transition in a thin rotating disc with inclusion*, Therm. Sci. 11(1): 103-118. doi: 10.2298/TSCI0701103G
27. Thakur P., Sethi, M., Gupta, K., Bhardwaj R.K. (2021), *Thermal stress analysis in a hemispherical shell made of transversely isotropic materials under pressure and thermo-mechanical loads*, ZAMM J Appl. Math. Mech. 101(12): e202100208. doi: 10.1002/zamm.202100208
28. Thakur, P., Sethi, M., Kumar, N., et al. (2021), *Analytical solution of hyperbolic deformable disk having variable density*, Mech. Solids, 56(6): 1039-1046. doi: 10.3103/S0025654421060194
29. Singh, N., Kaur, J., Thakur, P., Murali, G. (2023), *Structural behaviour of annular isotropic disk made of steel/copper material with gradually varying thickness subjected to internal pressure*, Struct. Integr. Life, 23(3): 293-297.

30. Sukhvinder, Gulial, P., Pathania, D.S., et al. (2024), *Comparative study of creep in a disk made of rubber/copper material and fitted with rigid shaft*, Struct. Integr. Life, 24(2): 159-166. doi: 10.69644/ivk-2024-02-0159
31. Singh, A., Gulial, P., Thakur, P. (2024), *Exploring the effective stress behavior of internally pressurized cylinders with varying density*, ZAMM - J Appl. Math. Mech. 104(8): e202400254. doi: 10.1002/zamm.202400254
32. Sukhvinder, Gulial, P., Pathania, D.S., et al. (2024), *Thermal stress distribution in a tube of natural rubber/polyurethane material and subjected to internal pressure and mechanical load*, Struct. Integr. Life, 24(2): 151-158. doi: 10.69644/ivk-2024-02-0151
33. Kumar, S., Thakur, P., Sood, S., et al. (2024), *Transversely isotropic elastoplastic behaviour in a mechanically loaded rotating disk*, Struct. Integr. Life, 24(2): 167-171. doi: 10.69644/ivk-2024-02-0167
34. Thakur, P. (2024), *Creep deformation in a thick-walled spherical shell having steady state temperature*, Struct. Integr. Life, 24(3): 301-304. doi: 10.69644/ivk-2024-03-0301
35. Thakur, P. (2024), *Analytical solution of bending sheet made of cast iron/bronze material*, Struct. Integr. Life, 24(3):305-307. doi: 10.69644/ivk-2024-03-0305
36. Gulial, P., Thakur, P. (2024), *Safety analysis in an elastoplastic orthotropic rotating cylinder under steady state temperature*, Struct. Integr. Life, 24(3): 309-313. doi: 10.69644/ivk-2024-03-0309
37. Sharma, A., Thakur, P. (2025), *Symmetry of rectangular plate made of isotropic material*, Struct. Integr. Life, 25(1): 39-41. doi: 10.69644/ivk-2025-01-0039
38. Thakur, P., Sharma, A. (2025), *Effect of non-homogeneity on the stresses and temperature distribution in a thick-walled circular cylinder*, Struct. Integr. Life, 25(1): 42-47. doi: 10.69644/ivk-2025-01-0042
39. Thakur, P., Gulial, P., Sharma, A. (2025), *Comparative elastoplastic analysis in a rotating disk made of polymer material with variable density parameter*, Struct. Integr. Life, 25(1): 48-52. doi: 10.69644/ivk-2025-01-0048
40. Gulial, P., Thakur, P. (2025), *Exploring steady-state creep deformation in an externally pressurized orthotropic rotating cylinder: a comprehensive investigation*, Int. J Appl. Nonlin. Sci. Online First. doi: 10.1504/IJANS.2025.10070431
41. Gulial, P., Thakur, P. (2024), *Exploring creep mechanisms in externally pressurized orthotropic cylinders with variable density*, Int. J Veh. Des. 96(3-4): 286-301. doi: 10.1504/IJVD.2024.146776